Infrared Thermography assisted evaluation of static and fatigue Mode II fracture toughness in FRP composites

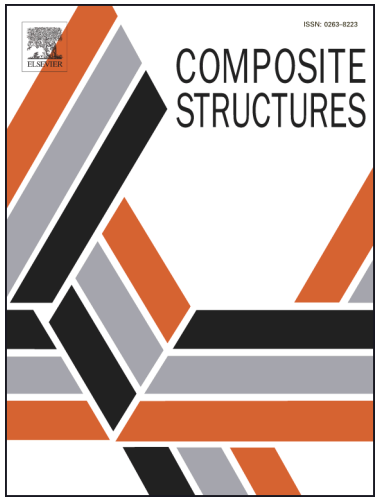

Infrared Thermography assisted evaluation of static and fatigue Mode II fracture toughness in FRP composites

Giuseppe Pitarresi, Tommaso Scalici, Giuseppe Catalanotti

PII: S0263-8223(19)31051-7
DOI: https://doi.org/10.1016/j.compstruct.2019.111220
Article Number: 111220
Reference: COST 111220

To appear in: *Composite Structures*

Received Date: 23 March 2019
Revised Date: 26 May 2019
Accepted Date: 9 July 2019

Please cite this article as: Pitarresi, G., Scalici, T., Catalanotti, G., Infrared Thermography assisted evaluation of static and fatigue Mode II fracture toughness in FRP composites, *Composite Structures* (2019), doi: https://doi.org/10.1016/j.compstruct.2019.111220

Infrared Thermography assisted evaluation of static and fatigue Mode II fracture toughness in FRP composites

Giuseppe Pitarresi[a,*], Tommaso Scalici[b], Giuseppe Catalanotti[c]

[a] *Dipartimento di Ingegneria - Università degli Studi di Palermo, viale delle Scienze Ed. 8, 90128 Palermo, Italy (giuseppe.pitarresi@unipa.it),*

[b] *Advanced Composites Research Group (ACRG), School of Mechanical and Aerospace Engineering - Queen's University Belfast, Belfast BT9 5AH, UK (t.scalici@qub.ac.uk)*

[c] *Advanced Composites Research Group (ACRG), School of Mechanical and Aerospace Engineering - Queen's University Belfast, Belfast BT9 5AH, UK (g.catalanotti@qub.ac.uk)*

Abstract

The work proposes the combined use of a Modified Transverse Crack Tension (MTCT) test coupon and Infrared Thermography, to evaluate the static and fatigue behaviour of Fibre Reinforced Polymer composites under Mode II delamination. Artificial delaminations starters are added to the TCT coupon, whose effects on the Strain Energy Release Rate are discussed. Infrared Thermography and Thermoelastic Stress Analysis are implemented to investigate stresses and delaminations growths on two FRP materials: a pre-preg IM7/8552 carbon fibre-epoxy and a glass-fibre reinforced epoxy laminates. The thermographic, thermoelastic and second harmonic signals have been determined and used to monitor the onset of instable crack growth under monotonic loading, and the delamination growth under fatigue loading. The use of such full-field non-contact thermographic parameters allows a further and effective insight on the behaviour of TCT specimens, providing useful information for the characterisation of the Mode II delamination behaviour under both static and fatigue conditions.

Keywords: Polymer Matrix Composites; Delamination Fracture Toughness; Mode II; Fatigue; Thermoelastic Stress Analysis.

Nomenclature

a	Delamination crack length
a_{th}	Threshold delamination length
A	Amplitude of the thermoelastic signal harmonic
B	Transverse Crack Tension specimen width
D	Amplitude of the Second-Harmonic signal
ext	sub-script for the strain measure by the extensometer
E	Young's modulus
E_x	Young's modulus measured by the extensometer at a certain growth of delamination cracks
G_{II}	Strain Energy Release Rate under Mode II
G_{IIc}	Critical Strain Energy Release Rate under Mode II
G_{II}^{ss}	Steady-state value of the R-curve
h	Thickness of the continuous plies skins

* Corresponding author.
Phone: +39 091 23897281. E-mail address: *giuseppe.pitarresi@unipa.it*

H	Total sample thickness
L	MTCT specimen length
L_g	Extensometer gauge length
N	Number of fatigue cycles
P	Phase of the thermoelastic signal harmonic
P	Applied tensile load
R	Stress ratio $\sigma_{min}/\sigma_{max}$
R-Curve	Material Resistance Curve
α	Coefficient of linear thermal expansion
σ	Stress. If no sub-scripts are added, it indicates the nominal far field stress in the TCT and MTCT samples
I,II	Sub-scripts indicating Mode I (opening tensile) and Mode II (in-plane shear).
1,2,3	Sub-scripts indicating the material principal directions
C-ELS	Calibrated End-Loaded Split specimen
CFRP	Carbon Fibre Reinforced Plastic
ENF	End-Notched Flexure specimen
GFRP	Glass Fibre Reinforced Plastic
FPZ	Fracture process zone
MTCT	Modified Transverse Crack Tension specimen
TCT	Transverse Crack Tension specimen
TSA	Thermoelastic Stress Analysis

1. Introduction

Knowledge of the static and fatigue interlaminar fracture toughness behaviour is essential to predict or prevent early failures in brittle layered structures and materials such as Fibre Reinforced Plastic (FRP) composites. The characterisation of the fracture behaviour is, in particular, required by design methodologies for primary structures. Regulations in the aerospace sector are trying to lighten up the *no-growth* conservative approach, based on preventing any crack growth under service loadings during the whole structure lifetime, in favour of a "slow crack" approach, where delamination growth, that can be monitored by defining appropriate inspection intervals [1–3], is tolerated within a certain extension. Any advancements towards a less conservative design would anyway rely on the accurate knowledge of the material fracture behaviour. This has fostered a demand for ever more robust and effective test methodologies, able to adequately assist the collection of data for the design stages [3,4].

Mode II interlaminar fracture is an important fracture parameter on its own. In fact, even if Mode II delamination usually requires higher energy than Mode I, there are a number of circumstances that see Mode II cracking as a favourite initiator and a main damage driving mode. These may include some typical structural cases: low velocity impact, ply-drop and splice joining sites in large composite panel assemblies [4,5], delaminations and crack tunnelling among layered structures such as fibre-metal laminates [6], delamination onset from bolted joint areas, where bolts pressure results in an out-of-plain opening constraint which rules out Mode I propagation [7].

The development of Mode II fracture evaluation procedures for FRPs has been significantly slower and more controversial than that for Mode I. Moreover, it has given birth to a number of different test configurations. An

evidence of the difficulties that have paved the way to accepted Mode II evaluation protocols is the only very recent release of standards, despite a long record of published research since early eighties. In particular, ASTM D 7905 and ISO 15114 have been made available in 2014, based respectively on the End-Notched Flexure (ENF) specimen, and the Calibrated End-Loaded Split (C-ELS) specimen. Still these long awaited standards are limited to static evaluation and the debate is instead open regarding extension to fatigue characterisation [8–11].

A simpler and more straightforward testing coupon for Mode II evaluation is the Transverse Crack Tension (TCT) specimen, also known as Central Cut-Ply (CCP), proposed since early nineties by DLR (Germany) researchers [12,13] and by Wisnom et al. [14–16].

The TCT is a beam specimen where a number of plies across the mid-plane are cut along the beam width thus forming a transverse crack (see Figure 1). Simple tensile loading is expected to be able to activate Mode II delaminations that, originating from the transverse crack tips, runs along the interface between continuous (i.e., outer skins) and cut plies. The use of the TCT specimen for the static evaluation of G_{IIC} is though not yet widely spread, as a number of issues, related with the complex local stress field introduced by the transverse crack, seem to be still not fully understood. The opportunity to evaluate values of G_{IIC} only after growing fatigue pre-cracks is also suggested in [13,17,18]. More recently, Scalici et al. [19] have presented a numerical and experimental study which shows that initial delamination in TCT samples is driven under mixed mode, up to a critical crack growth, a_c, after which a pure Mode II is fully settled. Furthermore, they also conducted a parametric study able to reveal that the driving force tends to a constant value, proportional to the applied load, after a certain threshold delamination length $a_{th}>a_c$. If the initial fracture process zone and amount of stable crack growth do not overcome such threshold crack length, a_{th}, there is a chance that unstable crack growth conditions are met not at the plateau of the material R-Curve, but at lower values, which may also vary for different materials and geometries. This may explain the size effects reported in [14,15]. Based on such findings, Scalici et al. [19] adopted a simple but effective modification of the TCT geometry, consisting of adding artificial interlaminar delaminations across the tips of the central transverse crack during manufacturing. Artificial crack lengths a_o longer than about 1.25 times the sample thickness H (see Figure 1a for dimensions definitions) are already able to overcome the adverse influences of the transverse crack zone, and activate a horizontal driving force curve (i.e. a driving force independent from the crack length). Under such conditions, the critical stress, i.e. the stress activating unstable crack growth, corresponds to the energy value at the plateau of the material R-Curve, i.e. the steady state fracture toughness.

The TCT coupon has also been used for fatigue characterisation, see e.g. Bergmann and Prinz [20], Ye et al. [13], Wisnom et al. [16], König et al. [17], Kawashita et al. [21], Allegri et al. [22], Rans et al. [18], and Daelemans et al. [23]. Some positive aspects arise about the use of the TCT specimen under fatigue cyclic loading:

- At a fixed load amplitude, and after the crack has grown over a threshold length (see above), the driving force G_{II} becomes constant, independent from the crack length, allowing to measure da/dN over a relatively high number of cycles;
- The delamination length and growth rate can be measured by simple, direct calibration compliance procedures using extensometers [21,22]. More advanced experimental stress and NDT analyses for the continuous monitoring of cracks could be implemented, exploiting the easier accessibility of the cycling TCT sample compared to the ENF or ELS coupons. See e.g. the work of Ribeiro et al. [24], using optical fibres, or the present

work and [19], proposing Thermoelastic Stress Analysis (TSA). In this regard, it is also interesting to quote some recent applications of IR Thermography and TSA to investigate similar tensile test coupons, embedding artificial delaminations but no transverse cut plies [25,26];

- The same sample can be subject to several blocks of load amplitudes (at constant stress ratio $R=\sigma_{min}/\sigma_{max}$), thus providing different values of da/dN vs. G_{II}, and reducing the number of samples to build Paris-like fatigue laws (since crack growth rates have been found to be independent from the sample load history [20]);
- Running blocks with decreasing load amplitudes and, hence, after the establishment of a natural fatigue delamination, should guarantee a finer determination of the threshold G_{II} value (see e.g. [13,17,20]). It is incidentally recalled how such threshold values are of primary importance in establishing appropriate design limits in *no-growth* design approaches;
- Compared to test coupons working in bending, simpler gripping fixtures are required. Moreover, the higher stiffness of the TCT specimen allows higher load amplitudes and smaller strokes, which can be optimally controlled by ordinary servo-hydraulic testing machines.

Following the work of Scalici et al. [19], the present work describes the results of static and fatigue tests on MTCT samples of Carbon Fibre Reinforced Plastic (CFRP) and Glass Fibre Reinforced Plastic (GFRP). In order to evaluate and monitor the stress behaviour and the delamination growth, both passive IR Thermography and Thermoelastic Stress Analysis have been implemented. The work, in particular, shows how the thermographic, thermoelastic and second harmonic signals all provide peculiar insights on the material behaviour, allowing to monitor the onset of instable crack growth under monotonic loading and the delamination growth under fatigue loading. Furthermore, the full-field maps of the thermoelastic signal, obtained in near-real-time from the front or edge sample faces, allow to estimate the delamination extension and shape, thus proposing TSA and MTCT as a powerful combination of tools for determining Mode II Paris-like fatigue laws for different FRP materials.

The paper is structured as follows: Section 2 provides a review of the data reduction scheme of a TCT sample and the expected behaviour for MTCT; Section 3 introduces the experimental setup, presenting in particular the passive IR Thermography and the Thermoelastic Stress Analysis methodologies in terms of hardware and signal processing; Section 4 and Section 5 describes the test results from the CFRP and GFRP sample materials. Both sections 4,5 follow the same structure: analysis of the features of the Thermoelastic Signal and correlation with the stress field, evaluation of the static behavior from monotonic tests, estimation of the fatigue Paris law. Due to the rather different thermographic and thermoelastic behavior of the two tested CFRPs and GFRPs, the two materials are presented separately, although the testing methodology are practically identical.

2. The Modified Transverse Crack Tensile specimen (MTCT)

Figure 1a shows a scheme of MTCT specimen. It differs from the TCT one for the introduction, during the manufacture process, of two release film inserts across the transverse crack tips [19,27]. Such artificial delaminations do not modify the data reduction leading to the formulation of the SERR, based on simple beam theory and evaluation of the change of specimen compliance with crack length a (see e.g. [13,17,22]). With reference to symbols reported in Figure 1a, the expression for G_{II} is:

$$G_{II} = \sigma^2 \frac{H}{4E_1}\left(\frac{1-\eta}{\eta}\right) \quad \text{with } \eta=\frac{2h}{H} \tag{1}$$

where E_1 is the Young's modulus along the fibres direction, σ the remote net-section stress field obtained by P/BH, where P is the applied load, B the specimen width, H and h the overall thickness of the specimen and the thickness of each bundle of continuous plies, respectively. The ¼ factor in Equation (1) arises from the presence of four delamination crack tips. According to [19], if the artificial delamination crack length is longer than a threshold value, estimated in about 2.5 times the specimen thickness for various degrees of orthotropy and η=0.5, then G_{II} is independent from a and proportional to the square of the remote tensile stress, σ^2 (hence proportional to P^2) according to eq. (1).

In the classic TCT sample scheme, the formation of a *fracture process zone* (*FPZ*), prior to instable crack growth, might not be sufficient to obtain a constant horizontal G_{II}. Instead, the MTCT will naturally meet the condition on the delamination length, if the artificial pre-crack is sufficiently long. With the MTCT specimen then a monotonic test in load control will see the driving force growing while staying horizontal (i.e. independent from a) as shown schematically in Figure 1b. By considering the intersection with a generic material R-curve (see Figure 1b), the accumulating elastic strain energy will give rise to an instable crack growth only when the driving force reaches the steady-state value of the R-curve, G_{II}^{ss}, i.e. when the tangency condition between the crack driving force and the R-curve is met.

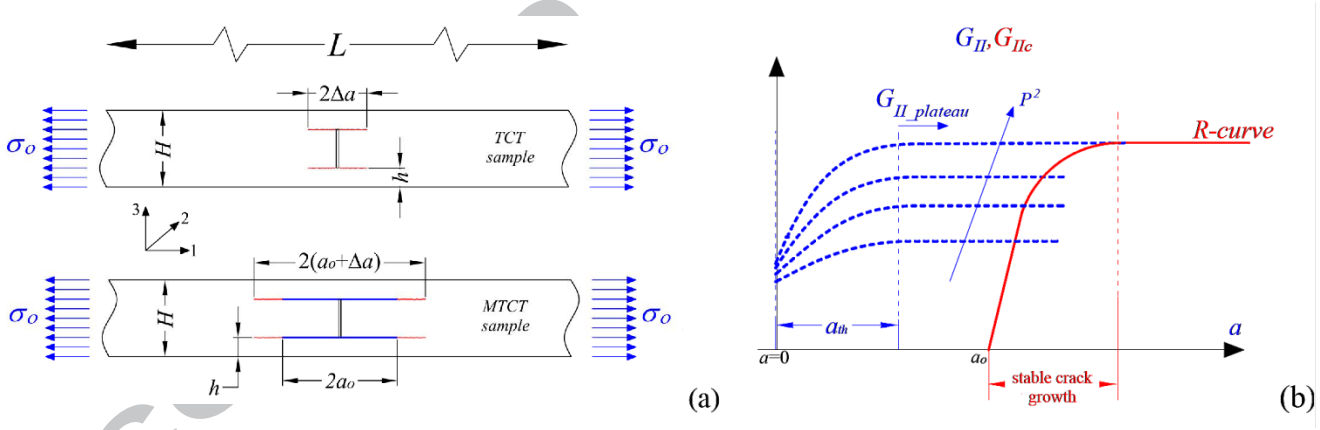

Figure 1. (a) edge-face sketch of a TCT and MTCT samples; (b) Schematic representation of a material Resistance Curve and Driving Force.

A certain amount of stable crack growth is always expected, due to the formation of the *FPZ*, and any possible toughening mechanisms increasing the material resistance [28]. In any case, such initial stable crack growth should not determine early load drops, but rather an increasing non-linearity in the load-displacement curve. It is also observed that the formation of a *FPZ* prior to instable growth is expected to determine a sharp natural crack front, which should reduce the influence of the thickness of the release film used for the artificial pre-crack. Cahain et al. [27] used the MTCT configuration to investigate the influence of insert films material and thickness. They found some slight variations in G_{IIC} with the film thickness but, interestingly, their measured values of G_{IIC} were also systematically higher than values from TCT samples. This seems to be in accordance with the interpretation of the flat driving force described above.

Regarding the use of the MTCT specimen for fatigue characterization, the presence of the artificial pre-cracks does not modify the material behavior, and fatigue cracks will naturally evolve from the pre-crack tips. It is here underlined that the presence of the artificial delaminations actually helps to prevent the formation of two un-symmetric delaminations fronts from the central notch. In the authors' experience, this event is rather frequent and generally prevents the successive synchronous activation of four delamination fronts, thus compromising the whole test. To avoid this, TCT samples require a careful preparation of the notch, with the cut plies accurately butted up and aligned to minimize local spurious effects. In this regard, the MTCT specimen is much less demanding and more robust, being practically insensitive to the overall quality of the central notch and resin pocket zone.

Extensometers have been used to monitor compliance variations and extrapolate the actual delamination length and its growth rate. The pre-crack in MTCTs will probably require longer extensometer gauge lengths, to include the initial delaminated zone. Compliance calibration is based on the following relationships, whose derivation is described in [13,22]:

$$a = \frac{L_g}{2}\left(\frac{\eta}{1-\eta}\right)\left(\frac{E_1}{E_x}-1\right) \text{ where } E_x = \frac{\sigma}{\varepsilon_{ext}} = \frac{P}{BH}\frac{1}{\varepsilon_{ext}} \tag{2}$$

$$\frac{\mathrm{d}a}{\mathrm{d}N} = \frac{E_1 BHL_g}{2P'}\left(\frac{\eta}{1-\eta}\right)\frac{\mathrm{d}\varepsilon'_{ext}}{\mathrm{d}N} \tag{3}$$

In Equations (2) and (3) L_g is the extensometer gauge length, and ε'_{ext} the strain measured by the extensometer at the load P'. During long running fatigue tests, it is more convenient to record values of peak and valley of the load cell and extensometer. Therefore, equation (3) is more useful to obtain directly the crack growth rate from the slope in time of the peak strains, detected at peak loads. Rans et al. [18] and Ribeiro et al. [24] have also found the use of equation (3) more reliable, since less prone to zeroing errors in the absolute evaluations of ε and P. It is important to mention that derivation of equations (1-3) requires the four delamination fronts to grow synchronously, i.e. they must mirror each other with respect to the mid-plane. The lack of such requirement could result in spurious flexural loads modifying the strain energy distribution among each delamination front. It is observed that, in general, the calibration compliance, obtained through equations (2) and (3), is somewhat "blind" against unsymmetrical crack growth, and will always handle a measure that, *ipso facto*, can be misleading. This can be a drawback in the use of TCT samples, and independent control of delaminations onsets and growths would be most useful to validate test data. This is done, in the present work, by means of IR Thermography (see Section 3.2 and 3.3).

3. Materials and methods

3.1. Preparation of CFRP and GFRP samples

Five unidirectional CFRP MTCT samples of Hexcel IM7/8552 have been obtained from a panel manufactured following the supplier's specifications. In particular, the Young's modulus E_1, estimated from the MTCT samples using an extensometer with gauge length of 100 mm centered on the initial delamination length, was 163±4 GPa, which is in accordance with data sheets from the supplier. The expected fibre volume for such material is about 60 %. It is also pointed out that the samples belongs to the same lot described in Scalici et al. (2016). Samples had

layup of $[0_8/\theta_{16}/0_8]$ (where θ indicates cut plies), and nominal dimensions of 300×15×4 mm^3. The release films placed across the transverse cut were 30 μm thick Teflon sheets, with width $2a$=40 mm.

Ten GFRP MTCT samples have been tested, five under fatigue loading and five under monotonic loading. The samples were cut from an in-house manufactured panel, assembled by hand lay-up and cured under vacuum bagging pressure. The panel employed a room temperature curing Epoxy Mates SX8 EVO and a unidirectional fabric made of glass yarns woven in the weft direction with low tex glass threads, having areal weight of 300 g/m^2. The lay-up was $[0_2/\theta_4/0_2]$. The final laminate achieved a fibre volume fraction of about 54 %, with a measured value of E_1=40.1±0.7 GPa. The rough surface finish left by the peel-ply fabric, used on both panel faces, decreased the material transparency, so that direct visual observation of the crack on the sample front face was not easy, nor reliable. Samples had final nominal dimensions of 300×15×3.4 mm^3, and the artificial delamination were made with a Fluorinated Ethylene Propylene (FEP) film of 13 μm thickness, cut to a width of $2a$=40 mm.

3.2. Experimental set-up

Samples were tested on an MTS 810 servo-hydraulic testing machine (MTS Systems Corporation), equipped with a 100 kN load cell and hydraulic MTS 647 grips. Deformations were measured by two HBM DD1 extensometers, with gauge length of 100 mm, mounted in twin opposite configuration (see Figure 2a). The two extensometers are wired such to measure the average strain from the two sides of the sample, thus compensating spurious bending. The extensometers were conditioned by the MTS digital controller, allowing to synchronize sampling with the load transducer. All monotonic tests were performed in load control at 2 kN/min while all fatigue tests were performed in load control, under constant load amplitude, at a load frequency of 5 Hz.

In order to allow free viewing access to the IR camera to acquire thermograms from both edge and front faces of the specimen, the grips were rotated at an angular position of 45° with respect to the testing machine inter-columns (see Figure 2b). The extensometer knives were rested against the sample front faces when acquiring thermograms on the edge face (see e.g. Fig 2a) and, vice versa, on the edge faces when acquiring on the front faces.

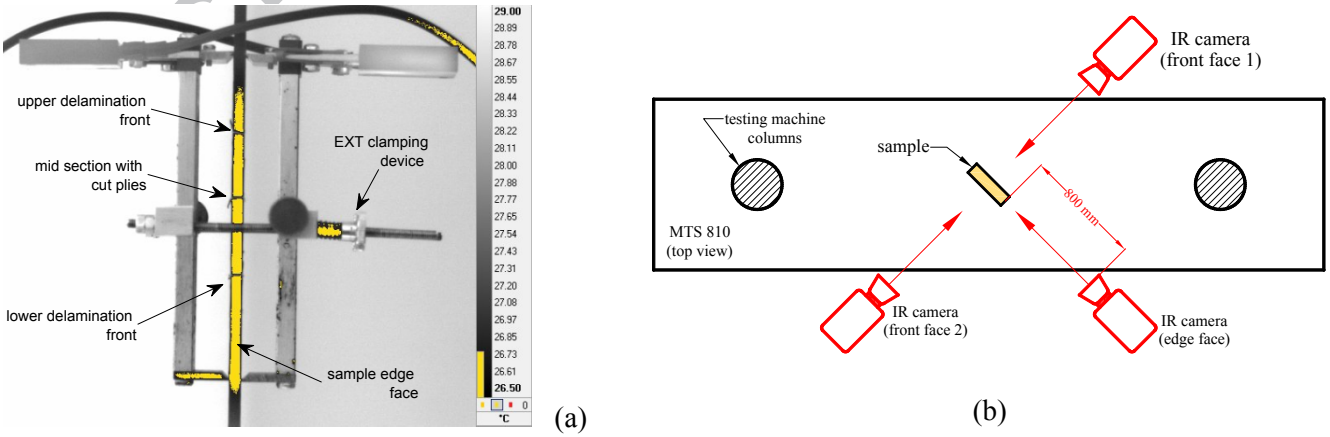

Figure 2. (a) sample with HBM DD1 extensometer in twin opposite configuration (IR image); (b) scheme of MTS 810 testing machine (base top view) with layup of the IR camera positions and specimen orientation.

IRT was used to acquire the full-field temperature and to implement TSA (see Section 3.3). The IR camera employed is a cooled sensor FLIR X6540sc (FLIR® Systems, USA), mounting a 50 mm focus lens allowing for a

Field-of-View (FOV) of 10.97°×8.78°. The IR camera was positioned facing either the sample width face or the sample edge face (see Figure 2b). Figure 2a is an example of edge-face view, where the visible marks at mid sample length, within the extensometer knives, indicate the position of the pre-crack tips and resin pocket and have been obtained by wrapping thin copper wires around the sample. Thermograms are acquired from a distance ranging between 400 mm (e.g. Fig. 3) and 800 mm, resulting in an Instantaneous FOV (size of one pixel on the specimen) of 0.12÷0.24 mm. The sampling frequency was 10 Hz for monotonic tests and 61 Hz for fatigue tests, with the integration time permanently set at 3000 μs.

Before testing, the analyzed surfaces have generally been coated with a thin layer of matt black paint, to uniform IR emissivity and reduce environment reflection disturbances. An exception was made for the GFRP front faces, which were left unpainted after verifying that they already had high emissivity and low IR reflectance, thanks to the peel-ply finish.

3.3. Thermoelastic Stress Analysis

TSA is a consolidated experimental stress analysis technique developed since the early eighties, based on the correlation between temperature changes and volume changes in linear elastic media deforming under adiabatic conditions (Thermoelastic Effect) [29]. Adiabatic behavior can be obtained by cyclic loading over a threshold frequency. The temperature change at the load frequency represents the thermoelastic signal, and for an orthotropic material it is correlated to the stress field by the following linear relationship [30–32]:

$$\Delta T = -T_o \frac{1}{\rho C_p}\left(\alpha_1 \Delta\sigma_1 + \alpha_2 \Delta\sigma_2\right) = -T_o \frac{\alpha_1}{\rho C_p}\left(\Delta\sigma_1 + \frac{\alpha_2}{\alpha_1}\Delta\sigma_2\right) \tag{4}$$

where T_o is the absolute temperature, ρ and C_p the bulk density and specific heat at constant pressure, respectively, α the coefficients of linear thermal expansion, and subscripts 1, 2 refer to the longitudinal and transverse material directions.

In TSA, it is customary to obtain the ΔT component of eq. (4) via a lock-in digital cross-correlation with a reference signal [33]. A sampling time window of a few tens of seconds is usually needed to achieve an effective filtering. In this work the amplitude and phase of the Thermoelastic Signal ΔT and the amplitude of the harmonic at twice the load frequency, called Second Harmonic, are both obtained using the FLIR® software THESA, which uses a physical reference signal at the load frequency. To further corroborate results, the sampled thermograms were also post-processed in Matlab, by applying the Discrete Fourier Transform on to the temperature *vs* time signal from each pixel [33]. This was actually obtained by means of the *fft* Mtalab® function. Both the THESA and Matlab® algorithms required just a few seconds to filter out the sought components. In particular, the TSA analysis applied in this work yielded the following three parameters:

- The Thermoelastic Signal absolute amplitude A;
- The Thermoelastic Signal phase P;
- The Second Harmonic amplitude D.

The time-sampling window used in all acquisitions in this work had a duration of 10 seconds. This was chosen after checking that longer times did not improve the filtered thermoelastic components. Furthermore, ten seconds were considered a sufficiently short time to assume negligible crack growth during the thermographic acquisition. Given the overall short time for acquisition and post-processing, TSA can be practically considered as a near-real-time monitoring technique in fatigue studies.

The map of phase *P*, under adiabatic conditions, discriminates zones where ΔT is in phase with the applied load with zones where ΔT is opposite in phase with the loading.

The presence of a Second Harmonic *D* term can be related to different thermomechanical phenomena. It can be associated to a dependence of material properties from temperature, as describe in the Second Order theory of the Thermoelastic Effect [34]. A number of dissipative phenomena have also been shown to determine irreversible temperature changes, variating twice per each loading cycle, and this has induced some researchers to associate the rise of *D* with the onset of dissipative phenomena (see e.g. [35,36]).

It is finally reported that no motion compensation was implemented in the evaluation of the thermoelastic signal. MTCT samples are rather stiff in their load direction, being this aligned with the fibers. Therefore, motion is entirely due to longitudinal elastic straining, which is relatively small and does not impair the use of the thermoelastic signal made in this work.

3.4. Plan of Experiments

Both CFRP and GFRP samples were processed according to the following steps:

- Monotonic_1.
  All samples were initially loaded in tension up to the break of the resin pocket present in the transverse crack. Such break was clearly identified in the extensometer and load cell signals, but also in the thermographic images. In order to obtain a better evaluation of the Young's modulus E_1, after the pocket failure the test was interrupted and restarted as Monotonic_2.
- Monotonic_2.
  Such tests were carried out up to delamination failure, in order to evaluate G_{IIC} for the virgin MTCT samples. Data for CFRP are in part taken from [19]. Data for GFRP are averaged from five tested coupons. During such tests the thermographic signal was acquired from the sample edge face, allowing to identify the instant of crack growth initiation.
- Fatigue.
  All fatigue tests were performed with load ratio $R=P_{min}/P_{max}=0.1$. Five GFRP and five CFRP samples have been cycled. During cycling the IR signal was acquired periodically, on time windows of 10 s. The acquired thermograms were then processed to obtain the Thermoelastic and Second Harmonic signals. Crack growths and growth rates were measured from the Thermoelastic data (see section 4), and compared with the values predicted by equations (2) and (3), based on the data from the extensometer. The obtained points of da/dN versus G_{II} were compared with data from the literature on similar systems.

- Monotonic_3.

  Monotonic tests performed on samples previously tested in fatigue. The previous fatigue tests were stopped after a crack growth between 5 and 15 mm. The Monotonic_3 tests were then performed up to failure, with the purpose to evaluate G_{IIC} on MTCT samples with fatigue grown crack fronts.

4. Results: CFRP

In this Section and in the next Section 5 the features of the thermoelastic signal are presented and commented first, as they are related to the stress field developed in the MTCT test coupon, for which some general considerations arise. The following sections are instead specific of the Mode II delamination toughness characterization. In particular, Sections 4.2 and 5.2 address the static behavior via the monotonic tests, and Sections 4.3 and 5.3 the fatigue behavior.

4.1. Thermoelastic Signal

Figures 3a,b,c,d show maps of A, P and D, obtained from the MTCT specimen edge surface, zooming on the upper delamination tips. The maps are obtained at the start of fatigue cycling, i.e. with no fatigue grown delamination, and are relative to sample CFRP #5 (loaded between 1.8-18 kN, see also Tab. 1).

The features of such A, P and D maps can be correlated with the stress field generated at t he crack tips. In order to do so, a schematic is reported in Figure 3e,f, where the two crack tips are indicated as A and B. The area a indicates the zone of internal cut plies, confined within the delaminations, i.e. behind the crack tips (wake of the crack). The area c still encloses the cut plies but is placed in the zone ahead to the crack tips. The area b lies upon the continuous plies ligaments. Within the area a it must be $\sigma_1=0$ as all load is transferred through the ligaments b. So the area a does not give rise to a transverse Poisson's contraction, $\varepsilon_3=-\nu\varepsilon_1$. On the contrary the area c must develop a $\sigma_1>0$ which will gradually grow along the longitudinal axis of the sample, up to the value of the remote tensile stress P/BH. Therefore, the traction stress in c will generate a Poisson's transverse contraction which will be hampered by the area a at the interface AB. This internal constraint will generate a transverse compressive stress $\sigma_3<0$ in a, counterbalanced by a transverse traction stress $\sigma_3>0$ in c (see Figure 3f). Here subscript 3 is used instead of 2, since the Cartesian coordinates on the sample edge plane are 1-3. In general 3 indicates the lamina out of plane direction, and the transversely isotropic nature of the UD laminas imposes that $\alpha_2=\alpha_3$. By recalling eq. (4), the sign of ΔT is given by the sign of the term $-(\alpha_1\sigma_1+\alpha_3\sigma_3)$. Let us assume that both CTS are positive, i.e. $\alpha_1>0$ and $\alpha_{2,3}>0$, with $\alpha_{2,3}$ typically significantly bigger than α_1 of an order of magnitude. Hence, the prediction of the sign of eq. (4) in the area a should provide:

$$\Delta T_a = -\frac{T_o}{\rho C_p}\left(\alpha_1 \underbrace{\Delta\sigma_1}_{=0} + \underbrace{\alpha_3}_{>0}\underbrace{\Delta\sigma_3}_{<0}\right) > 0 \tag{5}$$

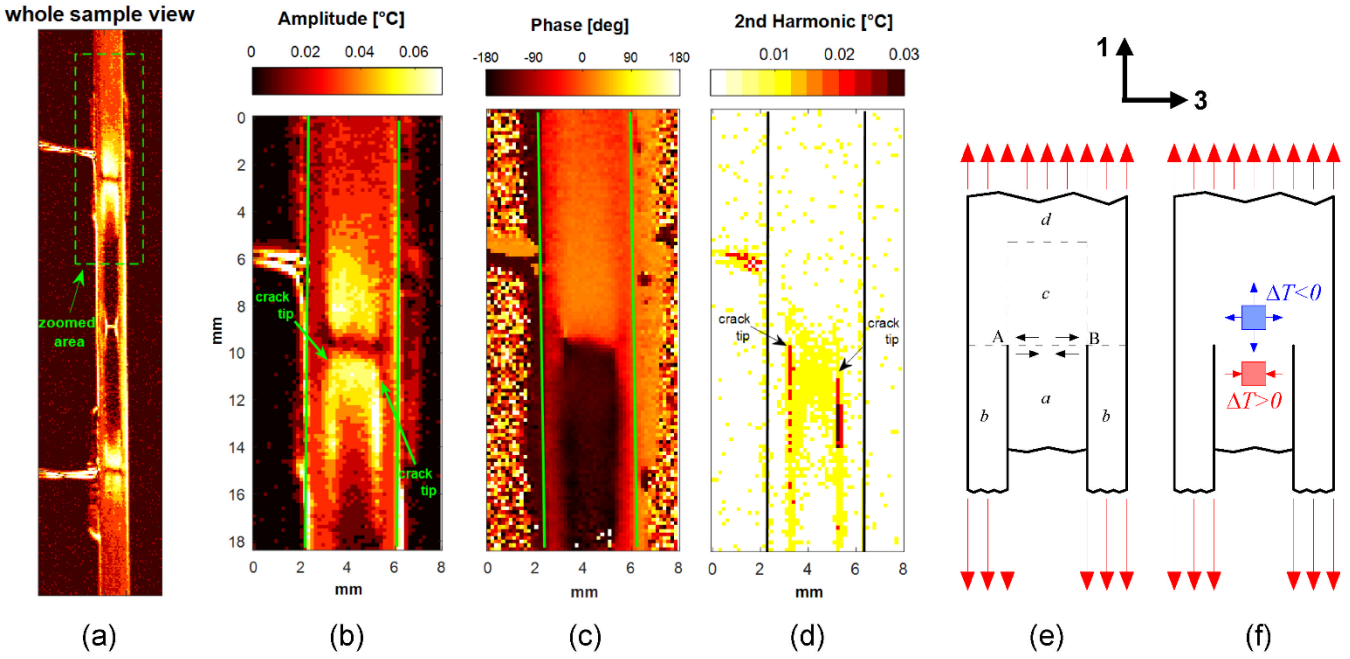

Figure 3: Maps of the thermoelastic signal around the top delamination tips: a) whole sample view; b) Amplitude *A*; c) Phase *P*; d) Second Harmonic *D*. e,f) schematic representations of the zone around the crack tips.

Considering now the area *c*, where σ_1 is different from zero and positive, the sign of ΔT_c is negative:

$$\Delta T_c = -\frac{T_o}{\rho C_p}\left(\underbrace{\alpha_1}_{>0}\underbrace{\Delta\sigma_1}_{>0} + \underbrace{\alpha_3}_{>0}\underbrace{\Delta\sigma_3}_{>0}\right) < 0 \tag{6}$$

This change in sign is indeed confirmed by the phase map in Figure 3c, which shows a 180° shift in phase between areas *a* and *c*. Since $\alpha_1 << \alpha_3$, the high thermoelastic signal shown in area c is likely due to the local rise of a σ_3 component, which must be positive in order to maintain the sign of ΔT_c negative, and therein be in accordance with the phase map result. It is also observed that σ_1 should become smaller while approaching the crack tips section, due to longitudinal stresses deviating towards the continuous plies (ligaments, areas *b*). In general, with CFRPs the assumption holds that areas of high thermoelastic signal are likely those with transverse stresses $\sigma_{2,3}$, as these are amplified by the α_3 coefficient [32].

When cyclic loading is applied, the assumption made in eq. (5) and (6) should imply that the temperature change is in phase with the applied load in area *a*, and in opposite phase to the load in area *c*. The phase map in Figure 3c is though insufficient to resolve the correct phase shift between the thermoelastic wave and the load wave. In order to find further experimental evidence of the above hypotheses, and resolve the phase uncertainty, some areas of the MTCT thermograms were analysed as indicated in Figure 4. In particular, Figure 4a shows a portion of the MTCT comprising the upper delamination crack tips and the threaded bar of the extensometer clamping rig (see also Figure 2a). Three sub-areas are selected to monitor their average temperature *vs* time during cycling. Sub-area *e* comprises a portion of the sample portion and a portion of the threaded bar, whose thermographic signal is much higher than the sample. In particular, when the load increases the specimen is pulled downward by the testing machine actuator, and the average temperature in sub-area *e* increases. Therefore, the average signal from area *e*

will be in phase with the load wave cycle. The other two monitored average temperatures come from a sub-area placed within area *a* (as defined in Figure 3d and 4a), and a sub-area within area *c*. As it is possible to see in Figure 4b, the temperature in area *e* is in phase with sub-area *a* and opposite in phase in sub-area *c*. From this comparison the previous uncertainty is resolved, and it is possible to conclude that area "a" is in phase with load wave while area "c" is in opposite phase, and both circumstances are possible only when $\alpha_1>0$.

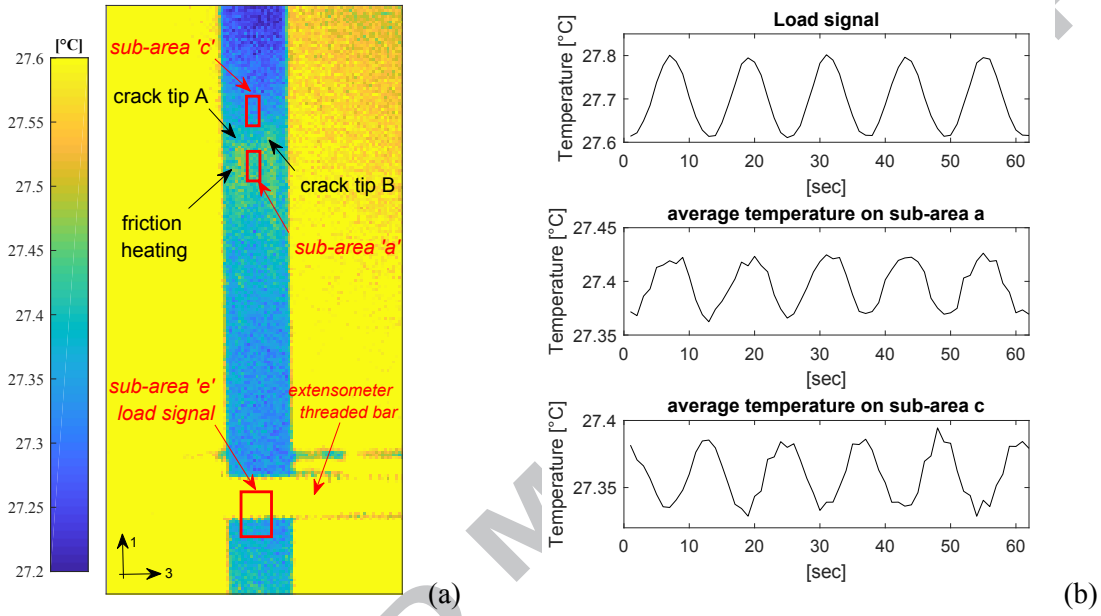

Figure 4. a) Thermogram showing the upper half portion of a MTCT sample during cycling; b) average temperatures acquired from the sub-areas defined in Figure 4a.

In the remote area *d* and in the ligament area *b* (see Figure 3e) there should be a prevalent mono-axial stress field, with $\sigma_3=0$ and $\sigma_1>0$. Therefore, in these areas it should be $\Delta T_{b,d}<0$, since $\alpha_1\sigma_1>0$. This should determine a phase value in areas *b* and *d* similar to the phase value in area *c*. From Figure 3c it is seen that areas *b* and *d* have a slightly shifted phase from that in area c. The causes of this slight out of phase signal are not clear. They might be the consequence of some spurious flexural deformations, which produce a through the thickness σ_1 stress gradient hampering the full onset of adiabaticity.

It is noticed that in eq. (4) the shear stress term τ_{13} is not present, and then there is no influence of such shear component on ΔT. This is indeed evident when considering the zones near the crack tips, were the presence of significant τ_{13} shears does not produce specific effects on the thermoelastic maps of Figure 3a,b,c. Therefore, the high thermoelastic signal present on the wake of the crack tips is mainly due to the transverse compressive stress component $\sigma_3<0$, arising as described above. This can be seen as an experimental confirmation of some previous numerical FEM results [15,19]. Moreover, the presence of such compression stresses would rule out any presence of mode I opening at the crack tips, thus leaving in-plane shear Mode II as the only possible cracking mode.

In Figure 3b, the crack tip section, i.e. the line AB, faces a narrow zone where the thermoelastic signal is low. Such a zone arises as a consequence of the gradual change of sign of σ_3 from negative, in area *a*, to positive in area

c. Such a narrow zone will follow the cracks during their growth, as long as the growth is the same for both delamination fronts.

Another interesting outcome from the present thermoelastic stress analysis is the presence of a higher second harmonic signal, right near the crack tips and along the delamination (see Figure 3d). By looking at the thermograms, it is believed that such high localized *D* signal is generated by dissipative heat due to sliding of the stretched ligaments over the central cut plies. The presence of the compressive stress σ_3 near the crack tips enhances this frictional effect, which is generated during each loading and unloading. Therefore, this dissipative term is modulated at twice the loading frequency, and hence detected through the second harmonic thermographic component. It is known that friction energy dissipation can influence the evaluation of the SERR [37,38]. It must be observed though that, in the present case, the second harmonic signal is very low (only a few hundredths of degrees), and the compressive stresses, being originated only by the internal constraint between the stretched and un-stretched portions of the cut-plies (see the explanation above), are expected to be much lower than that generated e.g. in ENF specimens. Furthermore, the frictional effect is enhanced by the fatigue cycling and is negligible in monotonic loading, as also observed by IRT.

The rise of such high second harmonic signal right on the wake of the crack, has been observed to follow the crack tip during it fatigue growth. Therefore, this thin mark of high *D*, visible in Figure 3d, can be regarded as a signature of the crack wake, and be exploited as another feature identifying the position of the delamination tips.

A final consideration is made about the lack of motion compensation in the present analysis. As shown in Figure 3a, the features of the thermoelastic signal amplitude shown in the upper delamination tips are pretty well replicated also in the lower delamination tips, and in general, the map shows good symmetry about the sample horizontal mid-section axis, confirming that motion is not disrupting the qualitative features of the signal as commented before.

4.2. Quasi-static tests

Quasi-static characterization was first preceded by Monotonic_1 tests, having the only purpose to break the resin pocket, i.e. the accumulation of resin in the transverse crack that still connects the cut plies. In all tested CFRPs such initial failure always occurred between 6-8 KN, i.e. well below the critical load at crack growth. The crack in the resin pocket was monitored by the IR camera staring at the sample edge face. The resin fracture was in particular evidenced by an intense, localized and brief rise of temperature, due to the sudden stress relief. Such signature of material break was localized around the transverse cut and therefore it could be concluded that there was no further damage affecting the zones near the delamination tips. This can be regarded as a further advantage of the MTCT configuration, since with classic TCTs the break of the resin pocket might easily trigger several local micro-fractures, influencing the successive delamination onset.

During Monotonic_2 tests (see Figure 5.a), thermograms of the edge face were acquired by the IR camera. This allowed to identify the instant of delamination onset, which was characterized by a sudden warm up of material along the delamination trajectory, due to the thermoelastic effect generated by the sudden load redistribution. Figure 5.b reports ten images of the sample edge face at successive time intervals before and after failure. The first image on the left is the thermogram before failure, and all others are acquired each every 0.1 secs from the

previous. Therefore, the second thermogram on the left is the closest after failure, and it is possible to notice the sudden warm up of all four delamination fronts. It is also seen that the temperature recovers its previous distribution during the next few seconds, and this can be interpreted as a confirmation that the temperature perturbation is due to the thermoelastic effect, activated by the load wave generated by the delamination. An avi file is made available as metadata which shows this sequence of thermograms at failure.

The above behavior was observed in all samples of Figure 5a, and allows to state that, for the present material type, the MTCT geometry exhibits a simultaneous reach of critical conditions in all four artificial crack tips. It is also observed that the delamination was always instable, with cracks growing all the way up to the grip zone. Neither the IR images nor the Load vs. Displacement curves showed signs of significant stable crack growth, even if the slight non-linearity of curves in Figure 5a is believed to be due to the formation of a *FPZ*. As indicated by Scalici et al. [19], the calculated value of G_{IIC}, i.e. 1.59±0.11 N/mm, is slightly higher than those reported in the literature, mostly based on ENF tests. This agrees with the statement that the MTCT provides the steady state G_{IIC}. A similar trend is reported also by Ye et al. [13] and König at al. [17] about a T300/914C CFRP. It is also noticed that the measured G_{IIC} compares well with the values found by Cahain et al. [27] on an MTCT specimen with inserts films with thicknesses ranging between 12 and 20 μm (against the 30 μm of this work).

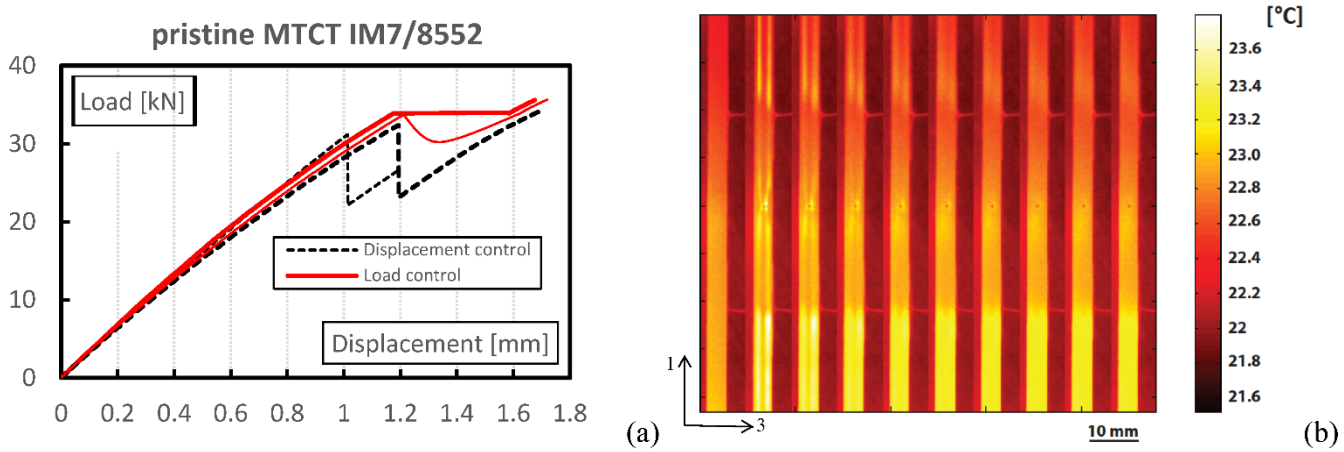

Figure 5. (a) Monotonic Load vs. Displacement curves for IM7/8552 samples with non-pre-cracked delamination tips; (b) sequence of thermograms acquired on the edge face, preceding and following the delamination.

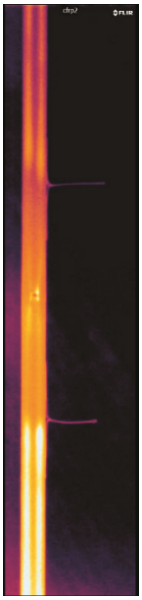

Video 1. Thumbnail link to video of thermograms at failure (same sample of Figure 5b). File provided as metadata.

Another noteworthy feature to report is that the delamination onset, as observed by IR Thermography, always coincided with the discontinuity in the Load vs. Displacement curves. Such curves, reported in Figure 5a, were obtained from tests performed in both load and displacement control. When displacement control was set, the discontinuity activated by the instable cracks growth presented a sharp drop in load. When load control is used, the discontinuity is followed by a local load plateau. In both cases, after the delaminations reached the grips zone, the samples were still able to sustain a new load increase, which was eventually interrupted by final catastrophic failure.

Figure 6a shows results of Monotonic_3 tests. Details on the fatigue grown cracks are reported in Section 4.3.

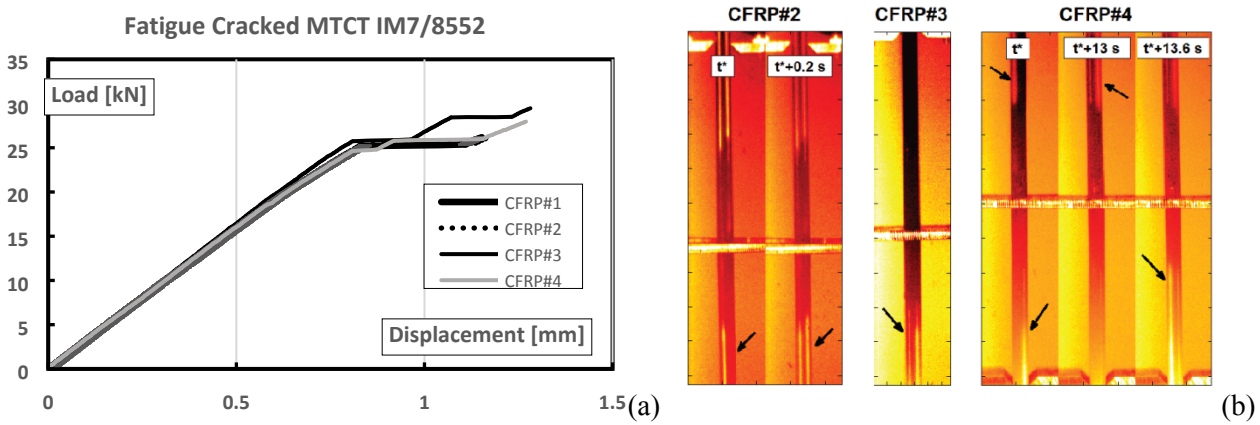

Figure 6. (a) Monotonic Load vs Displacement curves for IM7/8552 samples with fatigue pre-cracked delamination tips; (b) thermograms acquired on the edge face at the onset of delamination..

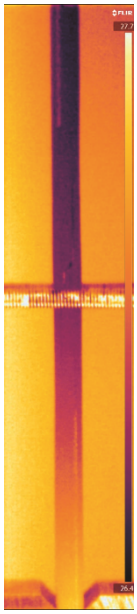

Video 2. Thumbnail link to video of thermograms at failure (same sample CFRP#4 shown in Figure 6b). File provided as metadata.

Compared to Figure 5a, the curves in Figure 6a appears to be straighter, and the absence of a more marked non-linearity can be related to the presence of a fully formed FPZ in the fatigue grown crack fronts. The critical loads obtained are though lower than those detected in Monotonic_2, resulting in a value of G_{IIC} of 0.94±0.04 N/mm.

The sequence of acquired thermograms allowed to discern clearly that delamination growth was now not simultaneous from all four crack fronts. This is in particular shown in Figure 6b, where some thermograms are reported of the various instants of non-simultaneous delaminations onset. By looking at the Load vs. Displacement curves, it is possible to find evidence of this behavior by observing the onset of a second plateau, followed by a new load increase before catastrophic failure. The horizontal plateaus between successive load growths are here obtained due to performing tests in load control. It is observed that, even if delamination onset was not simultaneous from all crack fronts, the new value of G_{IIC} has still a rather low dispersion, i.e. the first critical load is achieved at fairly similar levels in all tested samples.

The authors believe that the non-simultaneous growth can be due to differences in delaminations lengths and delamination fronts shapes after fatigue. In particular, it is suspected that each fatigue grown crack developed a slightly different FPZ and a somewhat non-uniform growth of the crack front along the beam width. Some authors have confirmed this, observing a somewhat irregular and concave crack front along the beam width [13]. A more recent numerical study by Hu et al. [39] also suggests a similar behavior.

In conclusion, the non-simultaneous reach of critical conditions is considered the main reason of the lower values of G_{IIC} obtained in Monotonic_3 compared to Monotonic_2. From the above observations, a critical aspect of the MTCT test arises: the reach of critical conditions at the four crack fronts is sensitive to local crack front conditions. The Load vs. Displacement curves, as obtained in both load and displacement control, may show some features which reveal a non-simultaneous crack growth. At this regard, it is noticed that some monotonic curves reported in Figure 3 from Kawashita et al. [21], relative to IM7/8552 TCT samples, show successive peaks after the

first drop. This could be a hint that instable delaminations are activated at different times, and might explain the computed lower value of G_{IIC} in [21] compared to Monotonic_2 values from this work. In any cases, IR Thermography has demonstrated to be is a useful remote full field technique to monitor the failure onset.

It is finally observed that [27] also reports values of G_{IIC} which are higher when measured from insert films, and lower when measured from fatigue grown cracks, or from TCTs with no artificial delaminations. According to what said in Section 2, the initial non-linearity of the driving force, G_{II}, in baseline TCT specimens, can be a cause for the onset of unstable crack growth at values lower than the steady-state value of the R-curve (see Figure 1b). A further cause that cannot be ruled out, according to the authors' experience, is the non-simultaneous activation of delaminations, which may be favored in the case of TCTs with a central irregular notch, or MTCTs with fatigue grown pre-cracks, due to higher exposition and sensitivity to local effects.

4.3. Fatigue tests

As described in Section 4.1, the features of the Thermoelastic and Second Harmonic signals could be used to monitor the evolution of crack growths under fatigue. Table 1 summarizes all information about samples tested. It is shown, in particular, that samples have been cycled in load control, at constant stress amplitude (R=0.1), with a value of σ_{1max} equivalent to a ratio G_{IImax}/G_{IIC} of 0.3 for four samples, and 0.37 for one sample, where the value of G_{IIC} used is the one obtained from Monotonic_2 tests.

The values of $\Delta a/\Delta N$ from TSA, shown in Table 1 relative to CFRP, are in particular taken from monitoring the trace of the Second Harmonic D signal. As mentioned earlier, the near wake of each crack generates a D signal that is attributed to frictional heating (see Fig. 3d).

Analyzing all the full-field thermoelastic maps acquired during the fatigue tests, it was possible to notice that, after an initial symmetric growth, the four crack fronts usually tended to evolve un-symmetrically, with one delamination side getting bigger than the other. The onset of such unbalanced condition was likely aggravated by the onset of spurious flexural loads, which hampered the regaining of a symmetric condition.

Figure 7 shows the last A and D maps, as obtained before stopping the fatigue cycling. These maps are also compared with the thermogram at failure, acquired from Monotonic_3 tests. The position of the crack tips as obtained from A and D agrees very well with that obtained from the thermogram at failure. It is also seen how sample CFRP#1 of Figure 7a developed a sensibly longer delamination on the left hand side.

The value of a used to compute the crack growth rate in Table 1 column 5 was the average from the four crack positions, while $\Delta a/\Delta N$ was obtained from a linear regression of a vs. N. The crack growth rate was also computed by means of eq. (2). This used the slope of the load vs. extensometer signal to obtain the value of E_x from monotonic tests performed at various intervals.

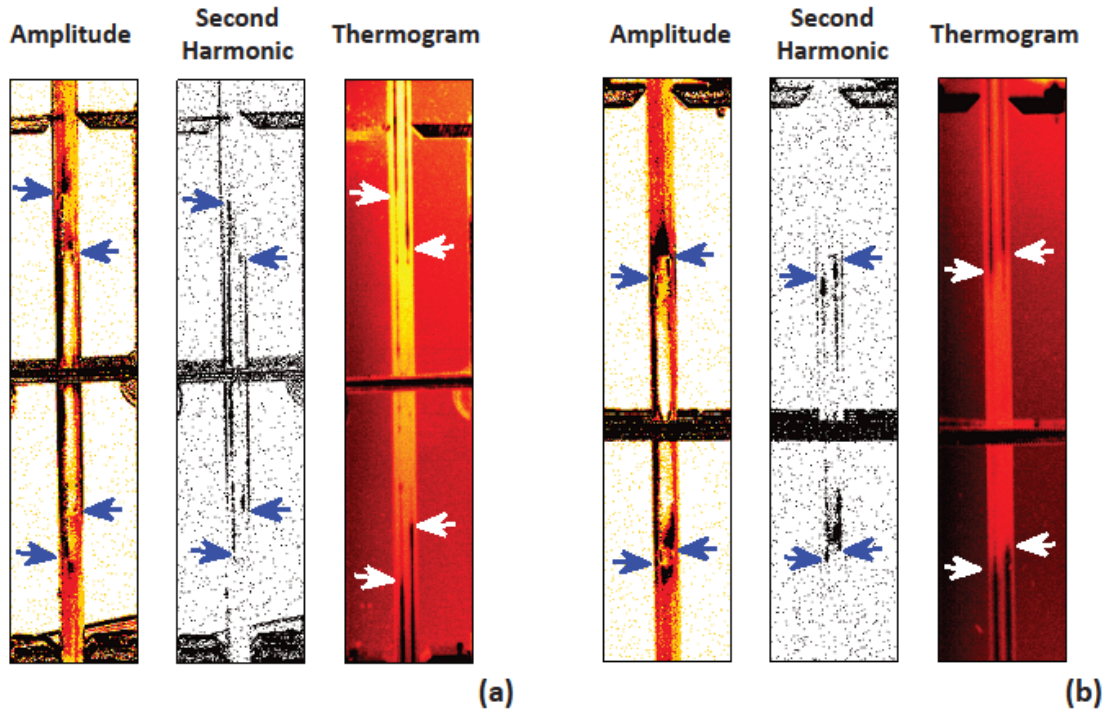

Figure 7. Comparison of maps *A*, *D* at the end of cycling and the thermogram at failure from Monotonic_3 test for: a) sample CFRP#1; b) sample CFRP#2. Arrows points to the position of each delamination tip.

Data in columns 4 and 5 of Table 1 are also compared with the empirical Paris-type equation from Allegri et al. [22] for the same material, IM7/8552, and the similar specimen type TCT. The same comparison is proposed in Figure 8, reporting the experimental data points obtained by Allegri et al. [22].

Table 1. Fatigue tests on IM7/8552 samples.

Material	$P_{min} \div P_{max}$ [KN]	N. of cycles	G_{IImax}/G_{IIc} [%]	$(\Delta a/\Delta N)_{EXT}$ (equation 2) [mm/cycle]	$(\Delta a/\Delta N)_{TSA}$ [mm/cycle]	$(\Delta a/\Delta N)$ * [mm/cycle]
CFRP #1	1.8÷18	18000	30 %	3.7E-4	4E-4	2.95 E-4
CFRP #2	1.8÷18	8500	30 %	3E-4	3E-4	2.95 E-4
CFRP #3	2÷20	2000	37 %	2.2E-3	2.2E-3	0.99E-3
CFRP #4	1.8÷18	14000	30 %	4E-4	2.7E-4	2.95 E-4
CFRP #5	1.8÷18	15000	30 %	//	3E-4	2.95 E-4

* Data based on eq. (11) and Table 2 coefficients from Allegri et al. [22].

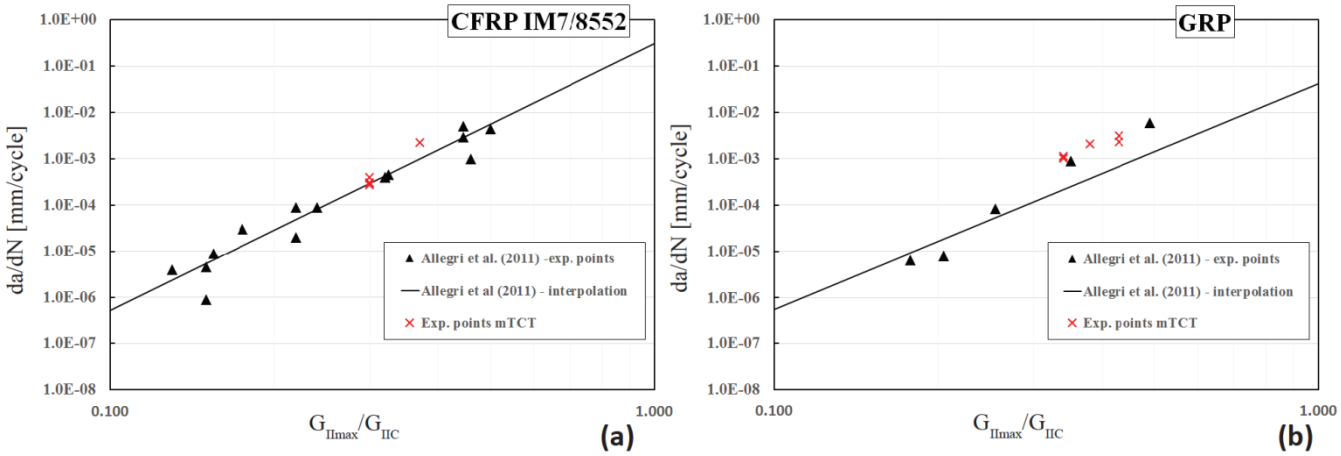

Figure 8. Comparison of experimental points obtained in this work with the Paris-law characterization from [22] for: a) IM7/8552 CFRP; b) GFRP.

5. Results: GFRP

5.1. Thermoelastic Signal

GFRPs generally have positive coefficients of thermal expansions along the principal material directions, i.e. $\alpha_{1,2,3}>0$. Moreover, the difference between α_1 and $\alpha_{2,3}$ is smaller than that of CFRPs, i.e. $(\alpha_2/\alpha_1)_{GFRP}<<(\alpha_2/\alpha_1)_{CFRP}$, and therefore the contribution of transverse stresses σ_3 to ΔT in eq. (4) is expected to be smaller [30,32]. Figure 9 provides an example of maps of A and P obtained from the GFRP samples tested in this work. As can be seen, the maps present some similarities and some differences if compared to the ones from to CFRPs. One similarity is the change of the sign of ΔT between areas a and areas b,c,d, which explains the 180° phase shift observed in the P maps. In fact, the sign prediction is the same reported by eqs. (5,6).

The presence of the 180° shift is a confirmation that the reciprocal constraint mechanism between areas a and c, described in details in section 4.1 is present also in GFRPs. A difference between GFRPs and CFRPs is instead the lack of a significant rise of the thermelastic signal in zones a and c, due to the σ_3 stress component. As mentioned before, this could be due to a smaller (α_2/α_1) ratio, but could also indicate a small value of σ_3. GFRP samples in this work have smaller thickness than CFRPs, and this could have reduced the constraint effect, giving rise to a smaller σ_3. It is noteworthy to report that the second harmonic maps, D, from GFRPs did not show any significant increased signal on the wakes of the cracks. Since friction dissipation is induced by the compression stress component σ_3, the lack of increase in D along the trace of the crack could be another hint that σ_3 is indeed lower in GFRPs.

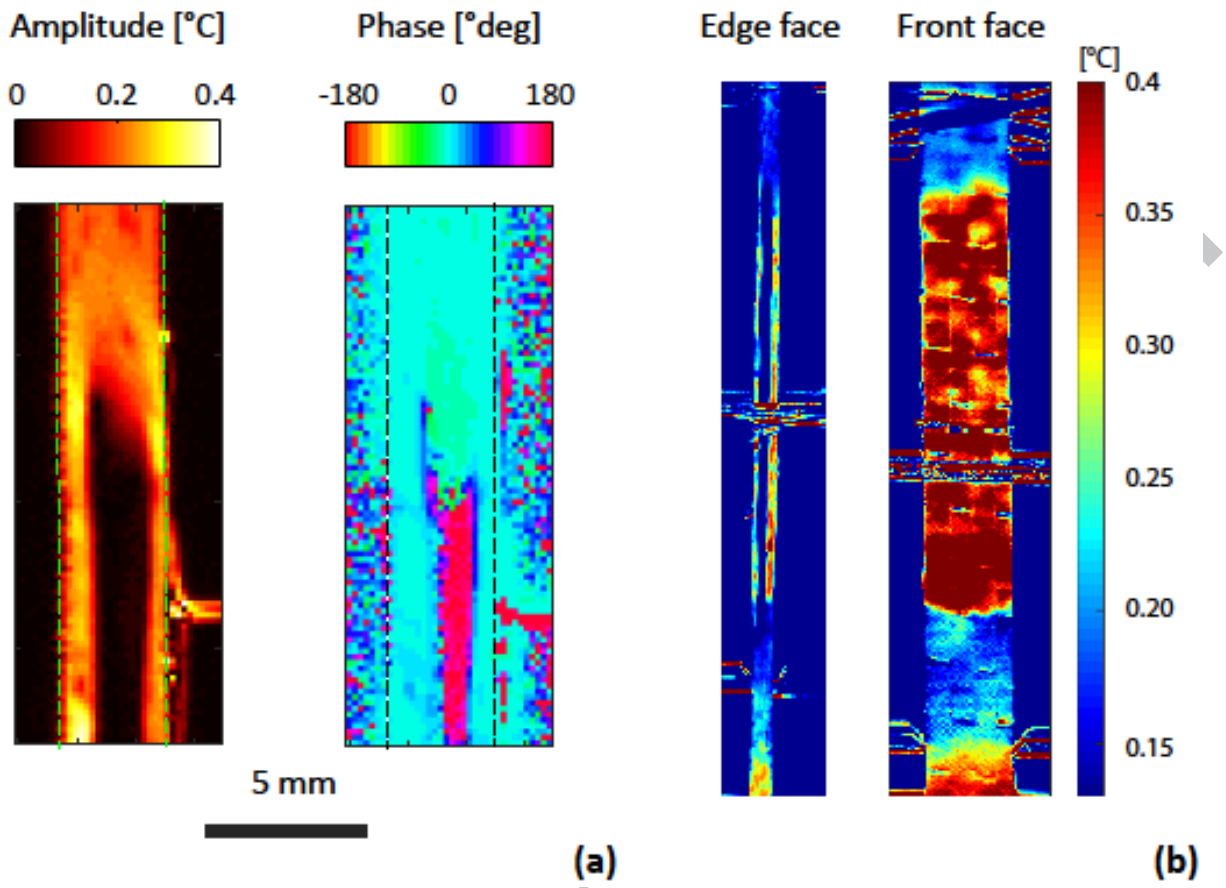

Figure 9. Thermoelastic signal in GFRP samples: a) typical A and P maps near the top delamination fronts; b) A map from edge and front face of a GFRP sample, after about 20 mm of fatigue cracks growth.

Thanks to the higher value of α_1, the thermoelastic signal in GFRPs is much more sensitive to the σ_1 component. In particular, it was found that the thermoelastic signal acquired from the sample front face is able to distinguish very well the area of delamination from the non-delaminated area. When the front face is analyzed, the delaminated area has a higher σ_1 component than the remaining non-delaminated zones, so the thermoelastic signal over the delaminated area is also higher. Figure 9b shows a comparison of the thermoelastic signal amplitudes measured from the edge and front face, in the case of a delamination that has already grown under fatigue by about 20 mm. As can be observed, TSA provides an excellent and rapid way to visualize the delaminated area. The boundary between low and high signal, is sharp enough to be easily traced. Furthermore, it is possible to observe that, in the case of GFRPs, the delamination front is usually maintained straight also during growth.

5.2. Quasi-static tests

Monotonic_1 tests showed that the breaking of the transverse crack resin pocket occurred between 3-5 kN, and no other failure or delamination onset was observed at this loads. Figure 10 reports Load vs. Displacement curves from Monotonic_2 and Monotonic_3 tests. In particular, three samples in Monotonic_2 were tested in displacement control, at a loading rate of 1 mm/min, while all other samples of both Monotonic_2 and Monotonic_3 were tested in load control, at a loading rate of 2 kN/min.

Figure 10a shows that the behavior at failure was pretty similar with both displacement and load control. Curves in load control were smoother, while curves in displacement control show a more irregular saw-teeth like aspect

during crack extension. One noteworthy feature of these curves is the lack of a clear identification of the onset of failure, as well as a fairly extended final portion of the curve characterized by a marked nonlinear load increase. This behavior is mainly due to a quasi-stable progression of the four delaminations branches, which exhibited a stick-slip behavior. It is in particular found that the transverse weft ties, which hold together the warp yarns in the glass fabric, act as local stoppers toward delamination, which has to regain extra energy to further progress. The meso-scale inhomogeneity introduced by the woven fabric is also responsible for a non-simultaneous onset and propagation of the four delamination fronts. IR-Thermography was once again very useful to reveal such stick-slip behavior. In particular, each delamination slip could be readily detected by a sudden increase of temperature over observed on both front and edge faces of samples.

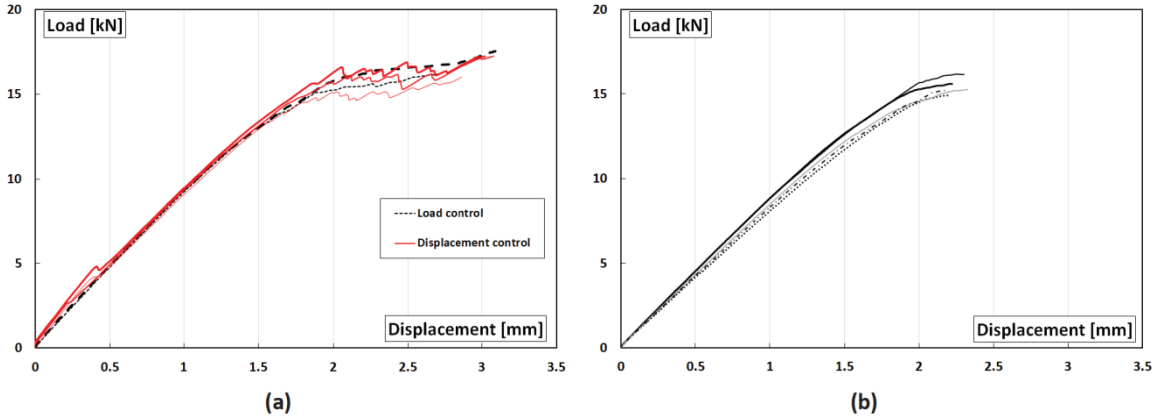

Figure 10. Load vs Displacement curves from: (a) Monotonic_2 and (b) Monotonic_3 tests.

Figure 10b shows results of Monotonic_3 tests, after a rather extended fatigue crack growth, of about 20 mm (see Section 5.3 for more details about fatigue cycling). The most noteworthy difference with curves from Monotonic_2 (Figure 10a) is the shorter extension of the nonlinear portion of the curves. This was due to the cracks being already very close to the condition of final catastrophic failure, having already grown by a consistent amount under fatigue cycles.

Figure 11 and 12 both illustrates how failure events could be detected by the IR camera. Figure 11 considers the sample front face, and the three thermograms shown report three delamination progressions in the zones indicated by the arrows. The correlation of these events with the Load vs. Displacement curve is also shown on the left hand side of Figure 11. Figure 12 shows the same correlation obtained from another sample observed from the edge face. In Figures 11 and 12 the transverse crack and of the delamination tips sections are marked by wrapping the sample with a thin copper wire (see also Figure 2). It is then possible to observe that the first delamination slips start from the initial delamination fronts, and then proceed with a stick-slip mode. Thermograms have in particular revealed that the start of delamination is seldom, if not never, simultaneous on all four fronts. This time such lack of synchronism is attributed to the slight different local toughness of the material, determined by the inhomogeneity at the mesoscale, introduced by the woven fabric. Fabric waviness and the curing process can both lead to the formation of non-uniform internal residual stresses which may affect the local fracture toughness. After the onset of delamination, the Load vs. Displacement curve progressively becomes less steep due to the increase of sample compliance.

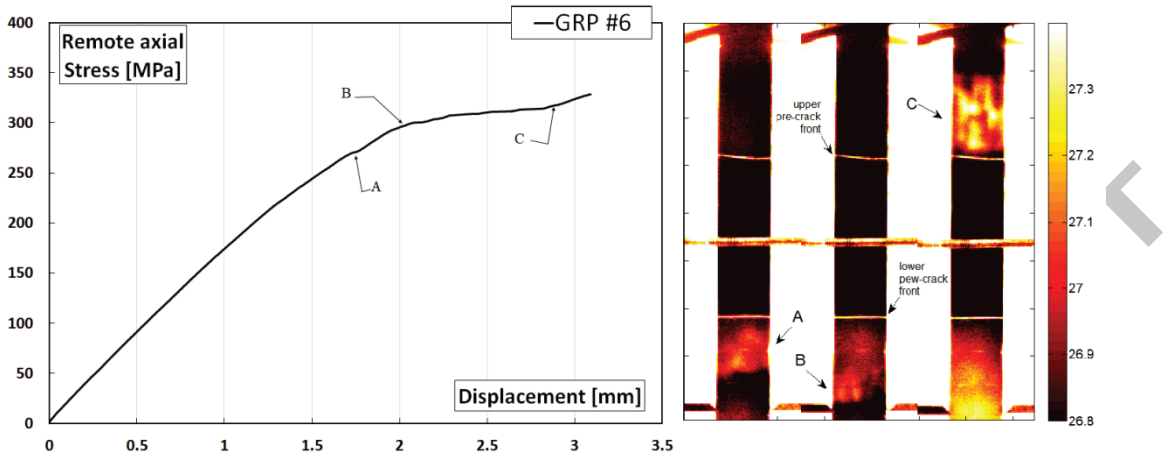

Figure 11. Correlation between delamination events and stress-displacement curve: monitoring on sample front face.

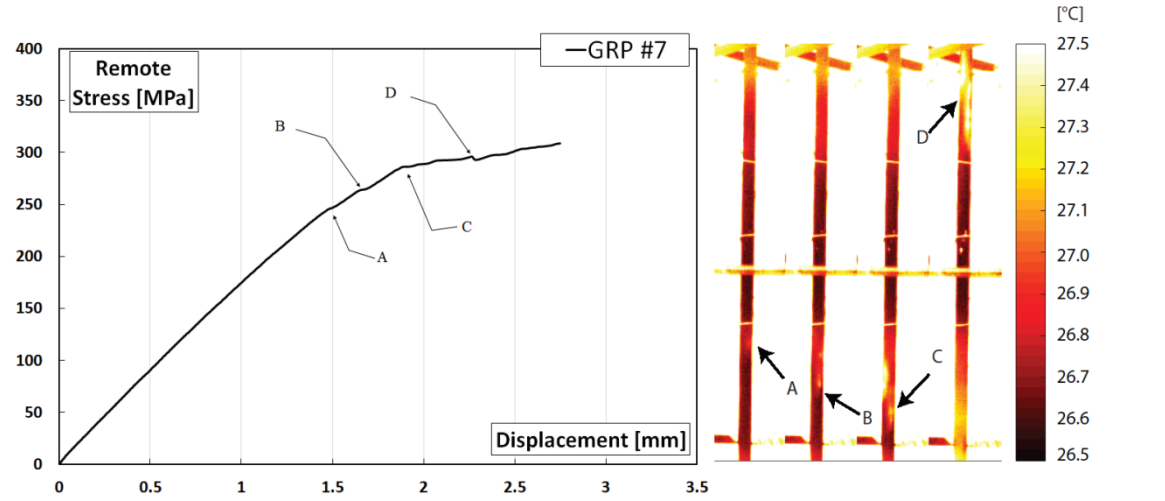

Figure 12. Correlation between delamination events and stress-displacement curve: monitoring on sample edge face.

In order to evaluate G_{IIC} for the GFRP material, the critical loads used in the calculation were those corresponding to the recording of the first delamination event, as observed from thermograms. The calculated G_{IIC} was averaged from all samples of both Figure 10a and 10b, and resulted in G_{IIC}=1.34±0.05 N/mm. Rather interestingly, as can be observed by the small standard deviation, such value of G_{IIC} now seems little influenced by the presence of a natural or artificial crack front. A possible explanation is that in GFRPs all delaminations grew fairly symmetrically. By the time fatigue cycling was stopped, all delamination fronts had grown a similar amount and the mismatches observed in CFRPs were now less marked.

5.3. Fatigue tests

Figures 13 reports thermoelastic maps taken from the front face of the sample during fatigue loading.

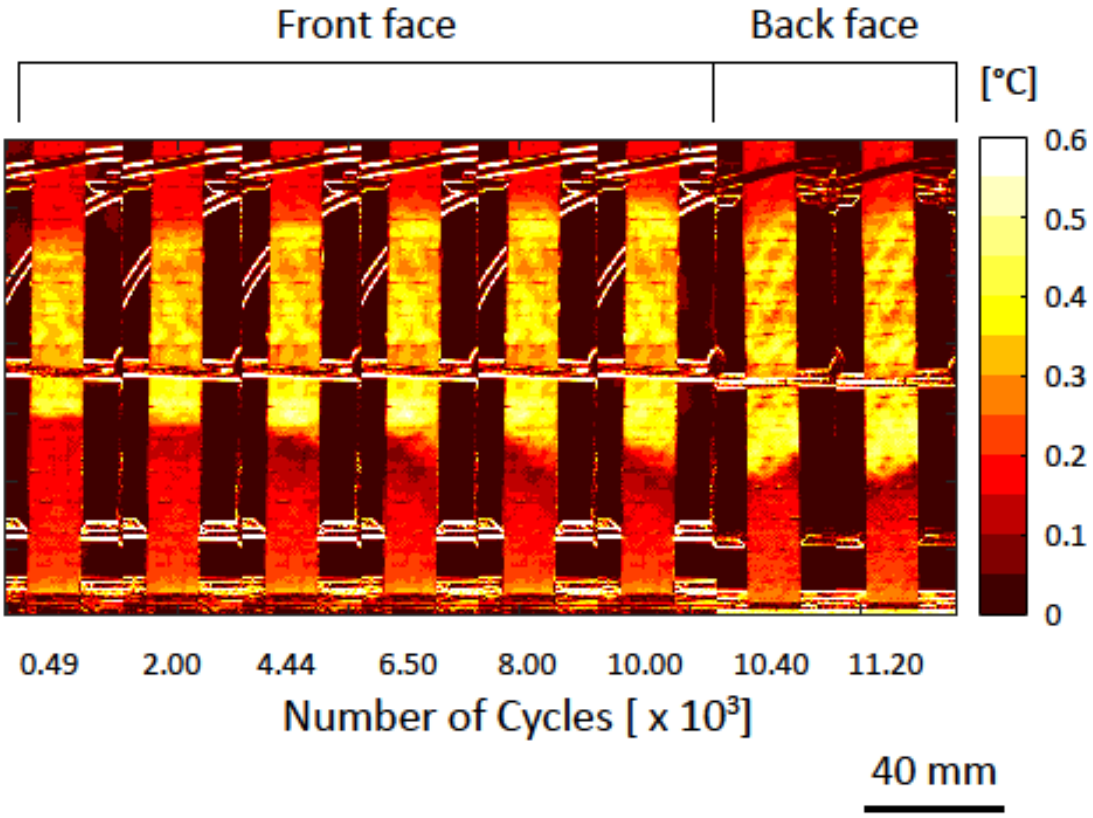

Figure 13. Maps of Amplitude (A) from the front faces of GFRP #2 at various steps of fatigue cycling.

In particular, it is seen that the front-face maps are very effective in evidencing the delaminated zone, as well as the shape of the delamination fronts. One potential drawback from using such setup is that only one delamination side can be efficiently monitored. This limitation may be dropped by using an infrared mirror to make the sample back face visible to the same IR camera [32].

Table 2 summarizes all data obtained from the fatigue tests. Values of $\Delta a/\Delta N$ were in particular obtained for three different values of G_{IImax}/G_{IIC}, with a loading ratio R=0.1.

Table 2. Fatigue tests on GFRP samples.

Material	$P_{min} \div P_{max}$ [KN]	N. of cycles	G_{IImax}/G_{IIc} [%]	$(\Delta a/\Delta N)_{EXT}$ (equation 3) [mm/cycle]	$(\Delta a/\Delta N)_{TSA}$ [mm/cycle]	$(\Delta a/\Delta N)$ * [mm/cycle]
GFRP #1	0.8÷8	7800	38	1.64E-03	2.13E-03	3.69E-04
GFRP #2	0.76÷7.6	12800	34	1.08E-03	1.13E-03	2.24E-04
GFRP #3	0.76÷7.6	12100	34	1.09E-03	1.04E-03	2.24E-04
GFRP #4	0.85÷8.5	3200	43	3.29E-03	3.14E-03	6.66E-04
GFRP #5	0.85÷8.5	4400	43	3.23E-03	2.29E-03	6.66E-04

* Data based on Equation 11 and Table 2 coefficients from Allegri et al. [22].

Form Table 2 it is seen that three values of $\Delta a/\Delta N$ are compared: the first value (Table 2, column 5) is obtained from the compliance calibration via the extensometer, the second value (Table 2, column 6) is obtained from identifying the delaminations fronts in the thermoelastic maps, and the third values (Table 2, column 7) are taken from [22]. The comparison between data from Table 2-column 6 and data from [22] is also proposed graphically in

Figure 8b. At this regard, it is here underlined that the GFRP material tested in this work and that considered in [22] are made with different fabric assemblies and manufacturing techniques, even if they have similar longitudinal Young's modules. Still the matching of the two sets of experimental data is close, and gives confidence that the Mode II fatigue behavior of GFRPs is fairly well predicted by the empirical model proposed in [22].

The prediction of $\Delta a/\Delta N$ via the calibration compliance (Table 2, column 5) was performed with the procedure using Eq. (3). In fact, the continuous use of the extensometer was now made more reliable by the higher compliance of GFRPs, and by the possibility to rest the extensometer knives against the thickness sides, with the application of a higher local pressure. Figure 14 shows the curves of the strain at peak versus the number of cycles. Some interesting features emerge from these curves. First, it is possible to identify an initial zone where the peak strain has a steeper growth. This behavior is believed to be due to the initial formation of a FPZ, at the starting of the fatigue cycling. This FPZ is created at a faster rate, and settles after a few hundreds of cycles. After this initial growth, the curves continue with a quasi-linear, less steep, gradient. It is, though, possible to observe that there is a slight fluctuation in the rate of evolution of such curves. This fluctuation is believed to be correlated to the inhomogeneity of the material at the mesoscale, primarily caused by the fabric assembly. The regular waviness of such fluctuations is probably associated to the delaminations crossing the regularly spaced weft ties. The values of $d\varepsilon'_{ext}/dN$, to be introduced in eq. (3) to yield $\Delta a/\Delta N$, are obtained from the linear regression of data, after removing the steeper first part of the curve. Even in the presence of the mild fluctuations, the linear regression provides a reasonable fitting, and the resulting values of $\Delta a/\Delta N$ compare well with those obtained from the thermoelastic signal (see Table 2).

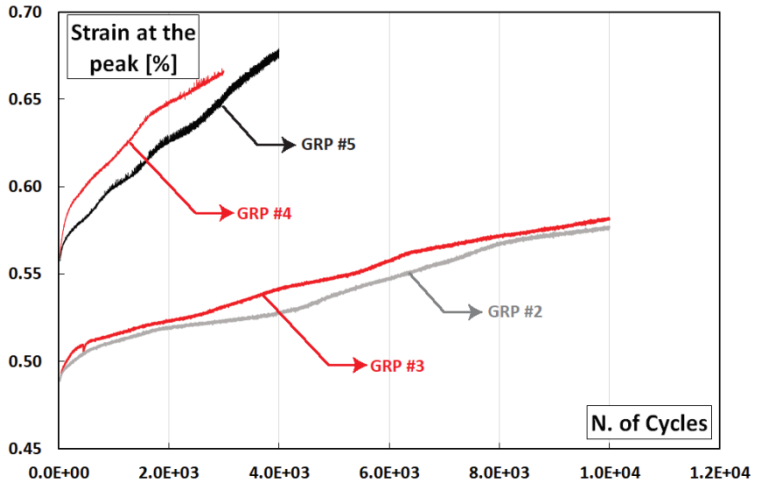

Figure 14. Curves of ε_{max}, measured by the extensometer at each peak load vs. the number of cycles (the slope of the curves corresponds to the derivate in equation (3)).

6. Conclusions

The proposed work has investigated the static and fatigue Mode II delamination behavior of Transverse Crack Tension specimens, using Infrared Thermography as a full-field non-contact technique for stress analysis and damage detection. The Transverse Crack Tension coupon considered has been modified by including interlaminar

delamination pre-cracks (MTCT), and the study has investigated specimens made of both carbon fibres (IM7/8552 pre-pregs) and glass fabrics, impregnated with epoxy resin by vacuum assisted resin infusion.

The work demonstrates the benefits of monitoring the temperature with focal plane array IR cameras, in full field non-contact mode, during both static and fatigue tests, to assist and enhance the characterization of the material. During fatigue loading, in particular, the sampling of thermograms has allowed to obtain the Thermoelastic and Second Harmonic signals, by means of a lock-in correlation data processing typical of Thermoelastic Stress Analysis.

The following is a list of major outcomes from this work:

- The presence of delamination pre-cracks in the MTCT test coupon eliminates the early influence of delamination length and initial mode mixity in the onset of critical delamination failure, allowing a direct measure of the steady-state critical Strain Energy Release Rate, G_{IIC}. Furthermore, the presence of pre-cracks reduces the sensitivity to local imperfections at the central notch, which may trigger unsymmetrical and asynchronous propagations of the four delamination fronts, in both static or fatigue tests;
- Temperature monitoring during monotonic tests is able to reveal the instants of crack propagation onsets. The elastic wave generated by load re-distribution after delamination onset generates a sudden temperature change that is readily detected by the IR camera, on both edge and front sample faces. This provides a useful insight on the activation of delamination. Moreover, in the case of GFRPs, the critical load could not be ascertained form the load-displacement curves measured during monotonic tests. In this case, analysis of thermograms allowed to identify the critical load for the evaluation of G_{IIc};
- The Thermoelastic Signal measured on the sample edge-faces of both CFRPs and GFRPs, during fatigue cycling, provides an evaluation of the stress field at the delamination tips. A qualitative interpretation of the thermoelastic signal reveals that the cut plies confined within the delaminations behave as an internal constraint against transverse Poisson's contraction, which generates local transvers stress components. Such thermoelastic maps show some peculiar features that can be exploited to monitor the evolution of the stress filed during fatigue crack growing, providing an immediate insight on the onset of un-symmetrical growth among the four delamination fronts. The thermoelastic maps also allow to estimate the position of the four delamination fronts independently, contrary to compliance methods using extensometers, which can provide only an average evaluation, without a direct insight of the real delamination scenario;
- CFRP samples have evidenced an increase of the Second Harmonic signal on the wake of each crack tip. Frictional effects, activated by transverse compression stresses, are identified as responsible for the generation of this signal. Such Second Harmonic trace, monitored during cyclic loading, proved to be a reliable signature of the position of the crack tips;
- In GFRPs, the higher sensitivity of the thermoelastic signal to the tensile stress component σ_1 determines an excellent signature of the delaminated zone on the map of the thermoelastic signal acquired from the sample front-face. Such maps provide also indications on the shape of the delamination fronts throughout fatigue growth.

In summary, the MTCT coupon is easily prepared and tested, since the required setup is the same as for routinely tensile tests. The use of Thermography, as proposed in this work, allows to evaluate damage onset and progression with a non-contact full-field and quick approach, avoiding the use of extensometers. These, on the other hand, are delicate sensitive which can be affected by pop-in like damages, such as the resin pocket fracture, and requires a post-processing analysis which can be slower than that required by TSA and passive thermography. Therefore, the authors believe that the MTCT coupon on one side, and the data rich thermographic evaluation on the other, could provide ideal conditions for performing Mode II evaluations in a more rapid and effective way.

Acknowledgements

The experimental activity has been carried out by using the IR thermal camera FLIR X6540sc, which has been purchased using funds from the project INTEP – PO FESR 2007/2013 – 4.1.2.A.

References

[1] Brunner AJ, Stelzer S, Pinter G, Terrasi GP. Cyclic fatigue delamination of carbon fiber-reinforced polymer-matrix composites: Data analysis and design considerations. Int J Fatigue 2016;83:293–9. doi:10.1016/j.ijfatigue.2015.10.025.

[2] Jones R, Kinloch AJ, Michopoulos JG, Brunner AJ, Phan N. Composites and the use of fracture mechanics data. Compos Struct 2017. doi:10.1016/j.compstruct.2017.07.097.

[3] Yao L, Alderliesten RC, Jones R, Kinloch AJ. Delamination fatigue growth in polymer-matrix fibre composites: A methodology for determining the design and lifing allowables. Compos Struct 2018;196:8–20. doi:https://doi.org/10.1016/j.compstruct.2018.04.069.

[4] Prieto L, Spenninger G, Wagner H. Experimental Determination of Energy Release Rate of Cfrp Structures by Means of Transverse Crack Tension Tests. In: Bos M, editor. ICAF 2009, Bridg. Gap between Theory Oper. Pract., Springer, Dordrecht; 2009, p. 513–28.

[5] de Vries TJ, Vlot A, Hashagen F. Delamination behavior of spliced Fiber Metal Laminates. Part 1. Experimental results. Compos Struct 1999;46:131–45. doi:https://doi.org/10.1016/S0263-8223(99)00049-5.

[6] Suiker ASJ, Fleck NA. Crack tunneling and plane-strain delamination in layered solids. Int J Fract 2004;125:1–32. doi:10.1023/B:FRAC.0000021064.52949.e2.

[7] Catalanotti G, Furtado C, Scalici T, Pitarresi G, van der Meer FP, Camanho PP. The effect of through-thickness compressive stress on mode II interlaminar fracture toughness. Compos Struct 2017;182:153–63. doi:10.1016/j.compstruct.2017.09.014.

[8] Carreras L, Renart J, Turon A, Costa J, Essa Y, Martin de la Escalera F. An efficient methodology for the experimental characterization of mode II delamination growth under fatigue loading. Int J Fatigue 2017;95:185–93. doi:10.1016/j.ijfatigue.2016.10.017.

[9] Brunner AJ, Stelzer S, Pinter G, Terrasi GP. Mode II fatigue delamination resistance of advanced fiber-reinforced polymer-matrix laminates: Towards the development of a standardized test procedure. Int J Fatigue 2013;50:57–62. doi:10.1016/j.ijfatigue.2012.02.021.

[10] Rans C, Alderliesten R, Benedictus R. Misinterpreting the results: How similitude can improve our understanding of fatigue delamination growth. Compos Sci Technol 2011;71:230–8. doi:10.1016/j.compscitech.2010.11.010.

[11] Sousa JA, Pereira AB, Martins AP, de Morais AB. Mode II fatigue delamination of carbon/epoxy laminates using the end-notched flexure test. Compos Struct 2015;134:506–12. doi:10.1016/j.compstruct.2015.08.002.

[12] Prinz R, Gädke M. Characterization of interlaminar mode I and mode II fracture in CFRP laminates. Proc. Inter. Conf. Spacecr. Struct. Mech. Testing. ESA SP-321, 1991, p. 97–102.

[13] Li Ye, Printz K, Klose R. Characterization of Interlaminar Shear Fracture Toughness and Delamination Fatigue Growth of Composite Materials Using TCT Specimen. Braunschweig, Germany: DLR-Interner Bericht. 131-90/15; 1990.

[14] Wisnom MR. On the Increase in Fracture Energy with Thickness in Delamination of Unidirectional Glass Fibre-Epoxy

with Cut Central Plies. J Reinf Plast Compos 1992;11:897–909. doi:10.1177/073168449201100802.

[15] Cui W, Wisnom MR, Jones M. An Experimental and Analytical Study of Delamination of Unidirectional Specimens with Cut Central Plies. J Reinf Plast Compos 1994;13:722–39. doi:10.1177/073168449401300804.

[16] Wisnom MR, Jones MI, Cui W. Delamination in composites with terminating internal plies under tension fatigue loading. ASTM Spec Tech Publ 1995:486–508. doi:10.1520/STP14031S.

[17] König M, Krüger R, Kussmaul K, Von Alberti M, Gädke M. Characterizing static and fatigue interlaminar fracture behavior of a first generation graphite/epoxy composite. ASTM Spec Tech Publ 1997;1242:60–81. doi:10.1520/STP18270S.

[18] Rans CD, Atkinson J, Li C. On the onset of the asymptotic stable fracture region in the mode II fatigue delamination growth behaviour of composites. J Compos Mater 2014;49:685–97. doi:10.1177/0021998314525482.

[19] Scalici T, Pitarresi G, Catalanotti G, van der Meer FP, Valenza A. The Transverse Crack Tension test revisited: An experimental and numerical study. Compos Struct 2016;158:144–59. doi:10.1016/j.compstruct.2016.09.033.

[20] Bergmann HW, Prinz R. Fatigue life estimation of graphite/epoxy laminates under consideration of delamination growth. Int J Numer Methods Eng 1989;27:323–41. doi:10.1002/nme.1620270208.

[21] Kawashita LF, Jones MI, Trask RS, Hallett SR, Wisnom MR. Static and fatigue delamination from discontinuous plies - Experimental and numerical investigations. ICCM Int. Conf. Compos. Mater., 2009.

[22] Allegri G, Jones MI, Wisnom MR, Hallett SR. A new semi-empirical model for stress ratio effect on mode II fatigue delamination growth. Compos Part A Appl Sci Manuf 2011;42:733–40. doi:10.1016/j.compositesa.2011.02.013.

[23] Daelemans L, van der Heijden S, De Baere I, Rahier H, Van Paepegem W, De Clerck K. Improved fatigue delamination behaviour of composite laminates with electrospun thermoplastic nanofibrous interleaves using the Central Cut-Ply method. Compos Part A Appl Sci Manuf 2017;94:10–20. doi:10.1016/j.compositesa.2016.12.004.

[24] Ribeiro F, Martinez M, Rans C. Evaluation of Mode Ii Fatigue Durability of Bonded Composite Repairs Using the Central Cut Plies. Meet Aeronaut Compos Mater Struct – MACMS 2015 2015:1–9.

[25] Kakei A, Epaarachchi JA, Islam M, Leng J, Rajic N. Detection and characterisation of delamination damage propagation in Woven Glass Fibre Reinforced Polymer Composite using thermoelastic response mapping. Compos Struct 2016;153:442–50. doi:10.1016/J.COMPSTRUCT.2016.06.044.

[26] Colombo C, Bhujangrao DT, Libonati F, Vergani L. Effect of delamination on the fatigue life of gfrp: a thermographic and numerical study. Compos Struct 2019. doi:10.1016/J.COMPSTRUCT.2019.03.023.

[27] Cahain YM Le, Noden J, Hallett SR. Effect of insert material on artificial delamination performance in composite laminates. J Compos Mater 2015;49:2589–97. doi:10.1177/0021998314550428.

[28] Anyfantis KN, Tsouvalis NG. Characterization of Fiber Bridging in Mode II Fracture Growth of Laminated Composite Materials. Adv. Exp. Mech. VII, vol. 24, Trans Tech Publications; 2010, p. 245–50. doi:10.4028/www.scientific.net/AMM.24-25.245.

[29] Pitarresi G, Patterson EA. A review of the general theory of thermoelastic stress analysis. J Strain Anal Eng Des 2003;38:405–17. doi:10.1243/03093240360713469.

[30] Pitarresi G, Conti A, Galietti U. Investigation on the influence of the surface resin rich layer on the thermoelastic signal from different composite laminate lay-ups. vol. 3–4. 2005.

[31] Emery TR, Dulieu-Barton JM, Earl JS, Cunningham PR. A generalised approach to the calibration of orthotropic materials for thermoelastic stress analysis. Compos Sci Technol 2008;68:743–52. doi:10.1016/j.compscitech.2007.09.002.

[32] Pitarresi G, Galietti U. A quantitative analysis of the thermoelastic effect in CFRP composite materials. Strain, vol. 46, Blackwell Publishing Ltd; 2010, p. 446–59. doi:10.1111/j.1475-1305.2009.00660.x.

[33] Pitarresi G. Lock-In Signal Post-Processing Techniques in Infra-Red Thermography for Materials Structural Evaluation. Exp Mech 2015;55:667–80. doi:10.1007/s11340-013-9827-1.

[34] Dunn SA, Lombardo D, Sparrow JG. The Mean Stress Effect in Metallic Alloys and Composites. Proc.SPIE, vol. 1084, 1989.

[35] Bremond P, Potet P. Lock-in thermography: a tool to analyze and locate thermomechanical mechanisms in materials and structures. Aerospace/Defense Sensing, Simulation, Control., International Society for Optics and Photonics; 2001, p. 560–6.

[36] Palumbo D, Finis R De, Ancona F, Galietti U. Damage monitoring in fracture mechanics by evaluation of the heat

dissipated in the cyclic plastic zone ahead of the crack tip with thermal measurements. Eng Fract Mech 2017;181:65–76. doi:https://doi.org/10.1016/j.engfracmech.2017.06.017.

[37] Amaral L, Zarouchas D, Alderliesten R, Benedictus R. Energy dissipation in mode II fatigue crack growth. Eng Fract Mech 2017;173:41–54. doi:10.1016/j.engfracmech.2017.01.020.

[38] Davidson BD, Sun X, Vinciquerra AJ. Influences of Friction, Geometric Nonlinearities, and Fixture Compliance on Experimentally Observed Toughnesses from Three and Four-point Bend End-notched Flexure Tests. J Compos Mater 2007;41:1177–96. doi:10.1177/0021998306067304.

[39] Hu YL, Carvalho NV De, Madenci E. Peridynamic modeling of delamination growth in composite laminates. Compos Struct 2015;132:610–20. doi:http://dx.doi.org/10.1016/j.compstruct.2015.05.079.